NANO LETTERS

Letter

pubs.acs.org/NanoLett

Nonequilibrium Structural Dynamics of Nanoparticles in $LiNi_{1/2}Mn_{3/2}O_4$ Cathode under Operando Conditions

Andrej Singer,*[,†] Andrew Ulvestad,[†] Hyung-Man Cho,[‡] Jong Woo Kim,[†] Jörg Maser,[§] Ross Harder,[§] Ying Shirley Meng,[‡] and Oleg G. Shpyrko[†]

[†]Department of Physics, University of California-San Diego, La Jolla, California 92093-0319, United States

[‡]Department of NanoEngineering, University of California-San Diego, La Jolla, California 92093-0448, United States

[§]Advanced Photon Source, Argonne National Laboratory, Argonne, Illinois 60439, United States

Supporting Information

ABSTRACT: We study nonequilibrium structural dynamics in $LiNi_{1/2}Mn_{3/2}O_4$ spinel cathode material during fast charge/discharge under operando conditions using coherent X-rays. Our in situ measurements reveal a hysteretic behavior of the structure upon cycling and we directly observe the interplay between different transformation mechanisms: solid solution and two-phase reactions at the single nanoparticle level. For high lithium concentrations solid solution is observed upon both charge and discharge. For low lithium concentration, we find concurrent solid solution and two-phase reactions upon charge, while a pure two-phase reaction is found upon discharge. A delithiation model based on an ionic blockade layer on the particle surface is proposed to explain the distinct structural transformation mechanisms in nonequilibrium conditions. This study addresses the controversy of why two-phase materials show exemplary kinetics and opens new avenues to understand fundamental processes underlying charge transfer, which will be invaluable for developing the next generation battery materials.

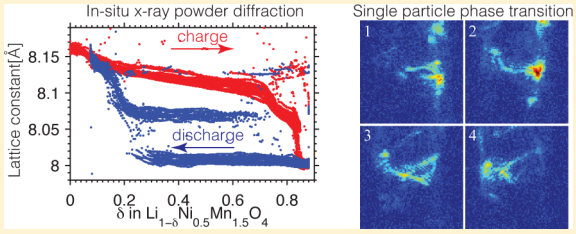

KEYWORDS: *Lithium ion batteries, operando, in situ, coherent X-rays, phase transformation, metastable solid solution*

Lithium ion batteries are ubiquitous in a wide range of technologies, including cell phones, electric vehicles, and sustainable energy systems,[1−4] and battery performance is inherently connected to the capability of lithium ions to reversibly intercalate with the electrodes.[5] Spinel materials show exemplary kinetics and are extremely appealing candidates for cathodes in future commercial batteries due to their specific energy, cost, availability, nontoxicity, and, importantly, high operating voltage.[6−9] Ion kinetics are governed by various nanoscale processes, including microscopic structural changes of the electrode.[10,11] The particular spinel of interest, disordered $LiNi_{1/2}Mn_{3/2}O_4$ (LNMO) is subject to multiple, fundamentally different sources of structural dynamics throughout the battery cycle: a cathode−electrolyte interface (CEI) layer can form due to high operating voltages,[12] strain due to inhomogeneous lithiation,[13] and the structure is known to coexist in two structural phases with different lattice parameters at particular lithium concentrations.[14−16] During battery cycling two-phase reactions compete with solid solution, which is beneficial for high rates in battery materials. Phase separation is unwanted for several reasons, such as a typically slow nucleation of a new phase,[17] diffusion limited transfer of lithium across the phase boundary,[18,19] and coherency strain in case of phase separation in individual particles, which leads to defect formation and capacity fade.[20,21]

Two-phase reactions are expected to yield slow kinetics, yet many high rate materials including $LiFePO_4$ (LFP), $Li_4Ti_5O_{12}$ (LTO), and LNMO experience phase separation during slow (dis)charge.[14,15,21,22] Several novel lithiation mechanisms were predicted to resolve this controversy, including domino cascade,[23] nonequilibrium kinetics,[17] and metastable solid solution, where concurrent two-phase and solid solution reactions occur.[20,24−26] As such, the interplay between solid solution and two-phase reactions is crucial for understanding the performance of the two-phase type battery materials. Here we report a direct observation of nonequilibrium structural dynamics, including the existence of a metastable solid solution, in spinel LNMO material using in situ coherent X-ray diffraction under operando conditions. We find that during charge the solid solution dominates in the beginning of the delithiation and even persists in the two-phase reaction region at low lithium concentrations. Interestingly, during discharge the cathode transforms via an extended two-phase reaction with no indication of solid solution, which occurs only after the two-phase reaction at very high lithium concentrations. The different transformation mechanisms indicate a remarkable hysteresis in the structural phase transformations.

Received: June 20, 2014
Revised: August 11, 2014

   dx.doi.org/10.1021/nl502332b | *Nano Lett.* XXXX, XXX, XXX−XXX

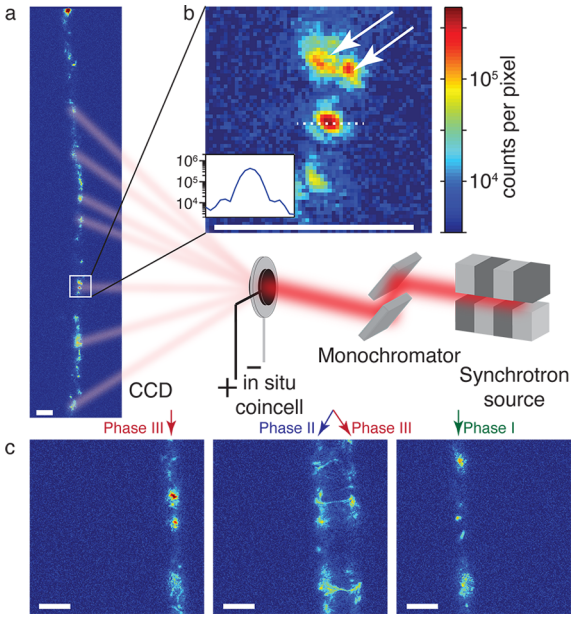

Figure 1. Experimental setup and measured diffraction patterns. X-ray radiation from the undulator is transmitted through a monochromator and is incident on a coin cell under operando conditions. (a) A portion of the Debye–Scherrer ring is recorded on a CCD. (b) An enlarged region of (a) shows fringes due to diffraction from a single cathode particle. (b, inset) Linescan through the white dashed line in (b). (c) Measured diffraction patterns for a lithium concentration of $1 - \delta = 0.12$ (left pattern), $1 - \delta = 0.7$ (center pattern), $1 - \delta = 0.9$ (right pattern) as in $Li_{1-\delta}Ni_{1/2}Mn_{3/2}O_4$. The arrows in (c) indicate different structural phases. All images are shown on the same logarithmic scale and with a scale bar of 0.1 nm^{-1}.

The experimental setup is shown in Figure 1. We acquired X-ray (9.0 keV photon energy) diffraction patterns in situ from an LNMO coin cell battery under operando conditions by a charge-coupled device (CCD) positioned at a distance of 0.5 m downstream of the sample. To transmit X-rays the coin cell casting had a 5 mm opening, which was sealed with a kapton film on both sides and did not mitigate the electrochemical performance. The sample was prepared with a disordered structure using the sol–gel method, similar to ref 8. The detector was shifted to a 2θ angle of 16.5° to record the (111) Bragg peak of the cathode, which contains randomly oriented individual nanoparticles. The incident beam size (200 × 200 μm defined by slits) and scattering geometry were chosen to observe 10–100 Bragg reflections from single nanoparticles on the detector. The crystallographic structure throughout cycling remains cubic (see Supporting Information Figure S1) thus the position of a single Bragg peak is sufficient to track the structural changes of the material.

A typical measured diffraction pattern is shown in Figure 1a, where several distinct Bragg reflections are observed along the Debye–Scherrer ring.[27] In the magnified image (see Figure 1b, center) interference fringes around the brightest spot indicate that indeed reflection from a single nanoparticle is recorded.[28,29] An analysis of the fringe period (see inset in Figure 1b) yields a particle size of 800 nm and concords well with observations from scanning electron microscopy (SEM) (see Supporting Information Figure S2). Some spots on the detector appear to be scattering from nanoparticles being not in the perfect Bragg condition (see arrows in Figure 1b). Diffraction patterns (about 600 in total) similar to those shown in Figure 1a,b were recorded, while the battery was cycled (see Supporting Information movie). Each image was collected in about 100 s and the maximum intensity between the strongest and weakest peaks in each image varies over more than 2 orders of magnitude. During charge and discharge various intriguing phenomena were observed, including continuous shifts and splitting of the Bragg peak. The former indicates a solid solution reaction with continuous change of the lattice parameter whereas the latter reveals a two-phase reaction, which is often considered as an emergent property of a many particle electrode.[30] Three images of the distinct phases are presented in Figure 1c.

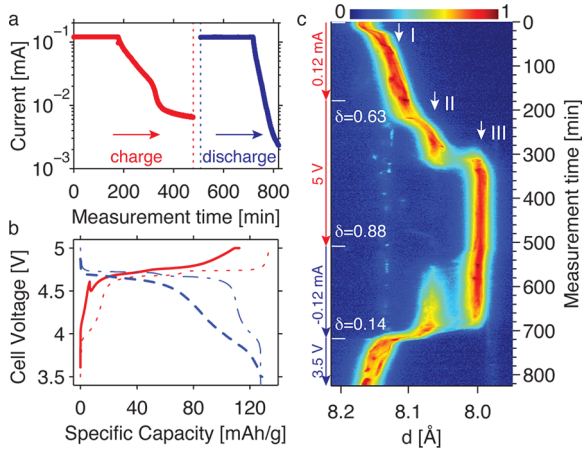

Figure 2. (a) Modulus of the applied current during charge and discharge as a function of measurement time shown on logarithmic scale. Between charge and discharge (vertical lines at about 500 min) we measured the open circuit voltage (OCV = 4.8 V). (b) Cell voltage versus Li/Li^+ as a function of specific capacity during charge (red solid line) and discharge (blue dashed line). The same curves for a 5 times slower cycling rate measured on another coin cell with the same chemical composition are also shown (red dotted and blue dash-dot lines). (c) The average along the Debye–Scherrer ring for all diffraction patterns shown on a logarithmic scale. Lithium concentration $1 - \delta$ as in $Li_{1-\delta}Ni_{1/2}Mn_{3/2}O_4$ and three different structural phases are indicated. Note that x-axis in (c) is reversed for easier comparison with Figure 1a and Supporting Information movie.

The electrochemical performance of the cell during the in situ X-ray measurements is presented in Figure 2a,b. The battery was charged with a constant current of 0.12 mA that corresponds to a C/4 rate (full charge in 4 h) and then held at a constant voltage of 5 V versus Li/Li^+ (see Figure 2a). During the discharge, a constant negative current of −0.12 mA (C/4, full discharge in 4 h) was applied and afterward the battery was held at a constant voltage of 3.5 V versus Li/Li^+. While held at a constant voltage the current is reduced as the intrinsic cell voltage approaches the applied voltage. Figure 2a indicates that lithium ion diffusion is significantly slower in the charged state, as compared with the discharged state.[18] The cell voltage deviates from the values recorded with a significantly slower cycling rate (C/20) due to polarization.[5] Although the battery was cycled prior to our measurements (2 cycles with C/4 and 100 cycles with 2C), the specific capacity of this particular coin cell battery reaches a value of 120 mAh/g, which is more than 80% of the theoretical capacity for this material (see Figure 2b).

To analyze the structural change of the whole ensemble of scattering particles we angularly averaged all diffraction patterns along the Debye–Scherrer ring and show this average as a

dx.doi.org/10.1021/nl502332b | Nano Lett. XXXX, XXX, XXX–XXX

function of measurement time in Figure 2c. As expected from ex situ measurements[14,15] (see also Supporting Information Figure S1) and theoretical calculations,[16] three structural phases are observed, which confirms that the spinel structure is disordered. These phases have a lattice parameter of 8.1 to 8.15, 8.08, and 8.0 Å and will be referred to as phase I, phase II, and phase III, respectively (see Figure 2c). Transitions between these phases are usually interpreted as reordering of the crystal structure due to Mn^{3+}/Mn^{4+}, Ni^{2+}/Ni^{3+}, and Ni^{3+}/Ni^{4+} redox reactions.[16,19]

During charge the lattice starts in phase I and shrinks due to extraction of lithium. It changes linearly with time in the first 200 min, indicating a solid solution reaction. The lattice constant decreases rapidly to phase II after 200 min. The Bragg peak splits after about 300 min, which marks the transition to phase III with simultaneous presence of two structural phases. Note that there is a drop in current and the slope of the curve in Figure 2a changes after 300 min, which indicates an increase in resistance of the material during its transition to phase III with a significantly slower ion diffusion.[18]

A reverse reaction is observed during discharge. The lattice expands and an extended two-phase reaction between phase III and phase II dominates for most of the discharge. Just after the completion of this phase transformation the structure abruptly jumps to phase I. Finally, a solid solution is observed for high lithiation.

Interestingly, the average in Figure 2c is not smooth but shows bright spots, which represent Bragg scattering from nanoparticles that perfectly satisfy the Bragg condition. The slightly different angles of these Bragg spots indicate some diversity in the behavior of nanoparticles, in particular during the solid solution transformation that occurs at high lithium concentrations. Different nanoparticles appear to have slightly different lattice parameters for the same charge state (0−200 and 700−800 min). Fluctuations in the Bragg peak intensity with time suggest that some particles change orientation during (dis)charge. A typical width of the Bragg reflection is about 0.02° and from the intensity fluctuations of these reflections in time we estimate that some nanoparticles can rotate slightly with a speed of less than 0.02° over a period of 10 min. Note that the rotation is significantly suppressed close to the fully charged state between 350 to 450 min, where the applied current is small (on the order of 0.01 mA). This indicates that particle movement is driven by charge transport. For highly charged states (200−700 min), we also observe a small fraction of reflections that correspond to the discharged state (see Figure 2c at d = 8.13 A) and appear to be disconnected from the charge transport. It is worth mentioning that the structure diversity among different nanoparticles and particle rotation cannot be captured in conventional XRD experiments that average over a much larger number of particles and yield a smoother distribution.

The most striking observation is the phase transformation between phase II and III with Bragg peak splitting, which starts after 300 min upon charge and again after 500 min upon discharge. This phase transformation is crucial to achieve full battery performance, and to better understand the interplay between solid solution and two-phase reactions we analyzed the positions of the Bragg peaks as a function of the lithium concentration, which was determined from electrochemical data (see Figure 3a). Figure 3a clearly shows that structural dynamics during charge and discharge are qualitatively different. The strength of the scattering signal corresponding

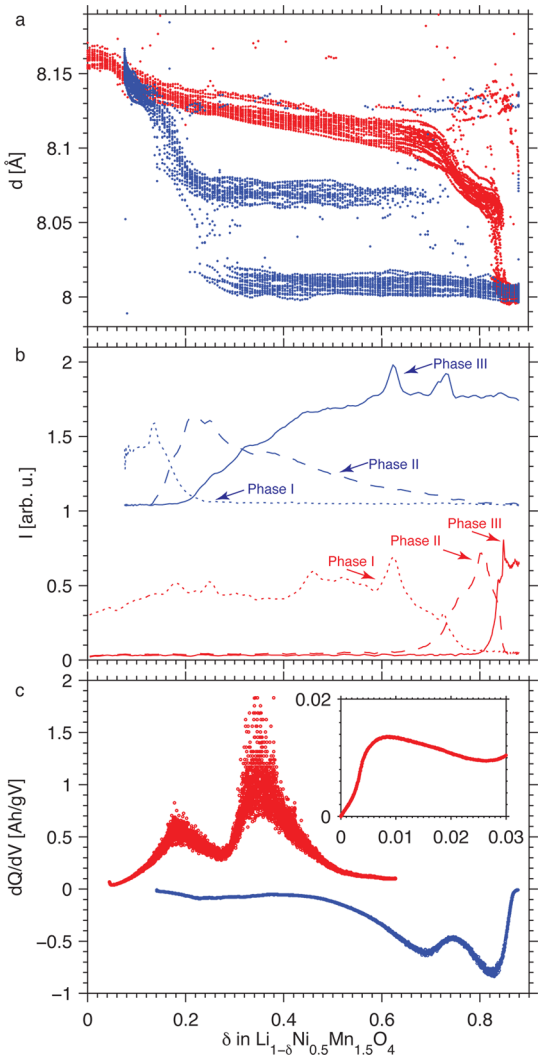

Figure 3. (a) Positions of the Bragg peaks as a function of lithium concentration found by dividing each diffraction pattern in 20 horizontal slices and fitting the projections of these slices with two Gaussian functions. (b) The scattering signal obtained by averaging Figure 2c horizontally in the range 7.98−8.05 Å (phase III, solid lines), 8.05−8.1 Å (phase II, dashed lines), and 8.1−8.2 Å (phase I, dotted lines). Discharge curves are displaced vertically for better visibility. (c) dQ/dV plot as a function of lithium concentration. The missing data at the end of the charge and discharge are due to the voltage holds. The data between δ = 0.03 and δ = 0.05 upon charge was compromised by polarization and is not shown (see Figure 2b). Inset of (c) shows an enlarged region. In all plots, red and blue colors represents charge and discharge, respectively.

to phases I, II, and III is shown as a function of the lithium concentration in Figure 3b. The hysteresis of the lattice parameter observed in Figure 3a,b is quite remarkable and is partially due to phase nucleation barrier and coherency strain, which both prevent a fast phase transformation.[5,31] But not only is there a hysteresis, our X-ray data also shows that solid solution dominates during charge, and an extended two-phase reaction prevails during discharge. Our X-ray data also indicates that the phase nucleation upon discharge occurs faster than upon charge.

To correlate structural dynamics with electrochemical data we present the latter as a dQ/dV plot in Figure 3c (Q is the total capacity and V is the cell voltage) where peaks correspond

dx.doi.org/10.1021/nl502332b | Nano Lett. XXXX, XXX, XXX−XXX

to plateaus in the coin cell voltage and are indicative of two-phase transformation under equilibrium conditions.[5] A comparison between the X-ray data and the electrochemical data during charge is quite surprising (see Figure 3b–d). Although we clearly observe peaks in the dQ/dV plot at δ = 0.01, δ = 0.2, and δ = 0.35, our X-ray data does not indicate any two-phase regions, which should reveal itself in Bragg peak splitting. The phase transformation eventually happens, but much later during the constant voltage hold at δ = 0.84. The material structurally appears to be in a solid solution regime, but electrochemistry suggests there is a two-phase reaction. Similar behavior has been observed in LFP using in situ X-ray diffraction data[32−34] and electron microscopy,[35] and we anticipate that this is a general phenomenon that occurs for two-phase materials during fast cycling. We also want to note that similar effects were theoretically predicted in LFP.[36]

We attribute the discrepancy between X-ray and electrochemical data to nonequilibrium structural dynamics due to the fast charge rate used in our experiment.[17] A possible explanation for the observed behavior is the fact that electrochemistry is governed by the surface of the nanoparticles, whereas X-ray diffraction is sensitive to their volume. Taking into account the smaller diffusion coefficient for charged (delithiated) material, as concluded from Figure 2a and ref 18, a comparison between electrochemical and X-ray data indicates that during charge (lithium extraction) the surface of the particle is actually delithiated, has a smaller lattice constant, and acts as an ionic blockade for ions trapped in the nanoparticles (see Figure 4). This layer forms at a voltage of about 4.7 V. No indication of this layer is observed in the X-ray diffraction signal, thus we conclude that this charge transport blockade layer is thin, provided it is as crystalline as bulk. The layer could also be blocking the electron transport, however, different ion diffusion coefficients for different structural phases suggest ionic blockade.

During discharge there is a reasonable correspondence between electrochemistry and X-ray diffraction of the nanoparticles (see Figure 3b–d). The dQ/dV plot shows three peaks and a close look at the structural information captured with X-rays reveals that there is indeed an abrupt lattice constant change, an appearance of an additional structural phase, and a transition to the third phase at δ = 0.83, δ = 0.7, and δ = 0.3, respectively. During discharge, the lattice transforms into a more diffusive material and there is no physical basis for an ionic blockade (see Figure 4), thus the electrochemical and X-ray measurements agree. The significant different behavior during charge and discharge renders CEI as an unlikely source of the dominant charge transport blockade, because CEI equally persists upon charge and discharge and builds up with cycling.[12]

Finally, a closer inspection of individual Bragg reflections during (dis)charge reveals structural dynamics of single nanoparticles. In particular, we analyzed the phase transformation between phase II and III after 300 min during charge and the back transformation after 500 min during discharge (see Figure 2c). We observe two simultaneous Bragg reflections connected by interference fringes, indicating they came from the same particle (see Figure 4) multiple times. This shows these particles are simultaneously in both structural phases and consist of domains with different lattice constants. The intensities of the respective peaks reflect the ratio of the two phases provided the entire crystal maintains the Bragg condition. Interestingly, during charge we also observe particles

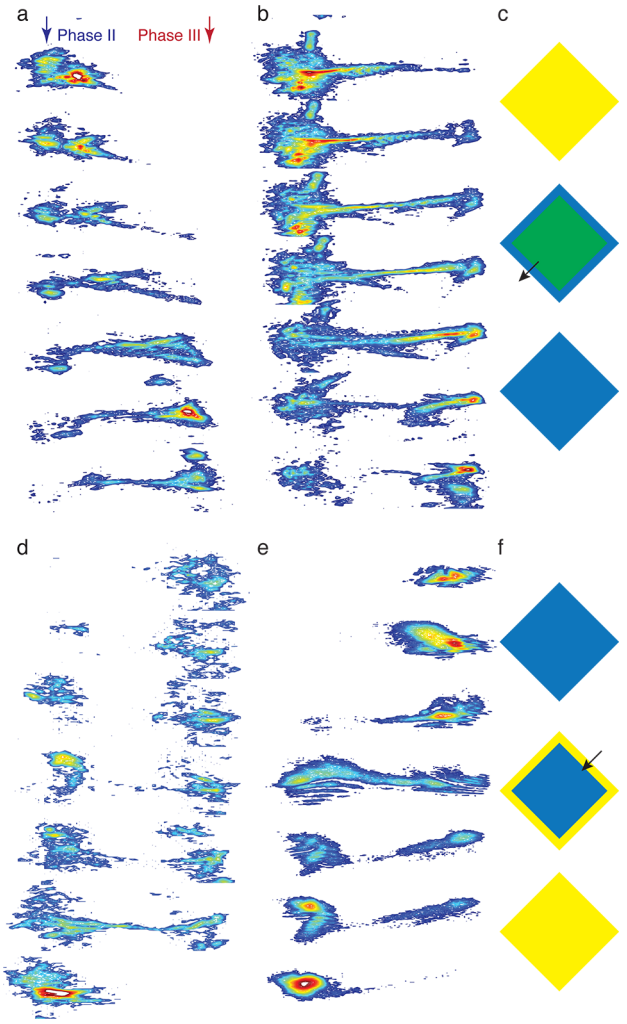

Figure 4. Phase transformation of different particles during charge (a,b) and discharge (d,e). Vertical axis is time and horizontal axis scattering angle (equivalent to lattice constant). Phase II and III are indicated. The time between consecutive images is 350 s (a,b) and 1000 s (d,e) and the first image (top) was recorded after 285 min (a,b) and 595 min (d). Different lithiation models for charge (c) and discharge (f). Yellow, blue, and green represent phase II, phase III, and solid solution between these phases, respectively. The direction of the lithium ion flow is indicated by the arrows. Data in (d) was collected in a separate measurement with a focused beam.

defying the traditional two-phase coexistence (see Figure 4a). Not only does the left peak (phase II) lose intensity and the right peak (phase III) gain intensity, there is a continuous shift of the maximum intensity during the phase transformation. This suggests a metastable solid solution mechanism,[20,24] where in the two-phase region one of the two phases (phase II here) undergoes a solid solution (see a sketch in Figure 4 and simulations in Supporting Information Figure S3). Another particle (see Figure 4b) shows similar behavior during charge with a slightly earlier phase transformation.

During the reverse phase transformation upon discharge we did not observe strong reflections between the two Bragg peaks corresponding to the two phases. This indicates no metastable solid solution, but rather a pure two-phase reaction, where the positions of the Bragg reflections are fixed (see Figure 4c). Note that the time scale in Figure 4c is increased by a factor of 3 as compared with Figure 4a,b to visualize the full phase

dx.doi.org/10.1021/nl502332b | *Nano Lett.* XXXX, XXX, XXX−XXX

transformation. To prove that we do observe phase transformation of single nanoparticles we performed additional measurements. We focused the beam to a size of a single nanoparticle (1 μm × 1 μm) and by scanning the sample assured that a single nanoparticle produced diffraction on the detector. We repeated the (dis)charge and before recording each diffraction pattern we carefully aligned the particle angle to maximum Bragg intensity, trying to compensate for possible particle rotations (see Figure 4d). Figure 4d shows two phases with fixed positions of the Bragg peak, is similar to Figure 4c, and confirms a pure two-phase reaction during discharge on this single nanoparticle. The same measurement was not possible during charge, because the phase transformation is considerably faster and the two-phase region is very narrow.

In summary, using coherent X-rays we were able to study nonequilibrium structural dynamics under operando conditions of a spinel structure lithium half cell. We mapped the structure on a single nanoparticle level and found that upon discharge the material shows an extended two-phase reaction, whereas during charge the cathode material mostly undergoes a solid solution reaction. A comparison of the X-ray data with electrochemical data measured simultaneously on the same operando battery suggests that during charge a thin ionic blockade layer is formed on the interface between cathode nanoparticles and electrolyte. This layer prevents faster charging, and no indication for such a layer is found for discharge. We anticipate that attempts to reduce the effect of the ionic blockade by doping the surface of the nanoparticles may lead to improved performance of battery material during fast charging. Finally, we foresee that the experimental in situ method developed here is ideally suited to study the interplay between solid solution and two-phase reactions for a large variety of next generation battery materials, such as LNMO, LFP, and LTO. We anticipate that it will ultimately open new avenues to understand fundamental processes underlying lithium ion kinetics and develop better battery materials.

■ ASSOCIATED CONTENT

Supporting Information

A movie of all in situ measured X-ray data, ex situ laboratory source X-ray diffraction data, scanning electron microscopy (SEM) images of the cathode material, and simulations of the Bragg reflection dynamics during a metastable solid solution reaction. This material is available free of charge via the Internet at http://pubs.acs.org.

■ AUTHOR INFORMATION

Corresponding Author

*E-mail: ansinger@ucsd.edu.

Author Contributions

A.S., A.U., Y.S.M., and O.G.S. conceived of the idea. H.M.C. and Y.S.M. prepared the samples. A.S., A.U., J.W.K., J.M., and R.H. performed the measurements. A.S. analyzed the data and wrote the paper. All authors participated in the interpretation of the data and revised the manuscript.

Notes

The authors declare no competing financial interest.

■ ACKNOWLEDGMENTS

This work was supported by U.S. Department of Energy, Office of Science, Office of Basic Energy Sciences, under Contract DE-SC0001805 and by the UCSD Chancellor's Interdisciplinary Award. H.M.C. and Y.S.M. acknowledge the financial support by U.S. Department of Energy, Office of Basic Energy Sciences, under Award Number DE-SC0002357. O.S. and Y.S.M. are grateful to the UCSD Chancellor's Interdisciplinary Collaboratories Award that made this collaboration possible. The use of the Advanced Photon Source, an Office of Science User Facility operated for the U.S. Department of Energy (DOE) Office of Science by Argonne National Laboratory, was supported by the U.S. DOE under Contract No. DE-AC02-06CH11357.

■ ABBREVIATIONS

LNMO: $LiNi_{1/2}Mn_{3/2}O_4$; LFP: $LiFePO_4$; LTO: $Li_4Ti_5O_{12}$; CCD: charge coupled device; OCV: open circuit voltage; SEM: scanning electron microscopy

■ REFERENCES

(1) Tarascon, J. M.; Armand, M. *Nature* **2001**, *414*, 359−367.
(2) Aricò, A. S.; Bruce, P.; Scrosati, B.; Tarascon, J.-M.; van Schalkwijk, W. *Nat. Mater.* **2005**, *4*, 366−377.
(3) Armand, M.; Tarascon, J.-M. *Nature* **2008**, *451*, 652−657.
(4) Dunn, B.; Kamath, H.; Tarascon, J.-M. *Science* **2011**, *334*, 928−935.
(5) Huggins, R. A. *Advanced Batteries*; Springer: New York, 2008; p 474.
(6) Deng, H.; Belharouak, I.; Cook, R. E.; Wu, H.; Sun, Y.-K.; Amine, K. *J. Electrochem. Soc.* **2010**, *157*, A447.
(7) Yang, M.-C.; Xu, B.; Cheng, J.-H.; Pan, C.-J.; Hwang, B.-J.; Meng, Y. S. *Chem. Mater.* **2011**, *23*, 2832−2841.
(8) Cho, H.-M.; Meng, Y. S. *J. Electrochem. Soc.* **2013**, *160*, A1482−A1488.
(9) Carroll, K. J.; Yang, M.-C.; Veith, G. M.; Dudney, N. J.; Meng, Y. S. *Electrochem. Solid-State Lett.* **2012**, *15*, A72.
(10) Balke, N.; Jesse, S.; Morozovska, A. N.; Eliseev, E.; Chung, D. W.; Kim, Y.; Adamczyk, L.; García, R. E.; Dudney, N.; Kalinin, S. V. *Nat. Nanotechnol.* **2010**, *5*, 749−754.
(11) Zhu, J.; Lu, L.; Zeng, K. *ACS Nano* **2013**, *7*, 1666−1675.
(12) Duncan, H.; Abu-Lebdeh, Y.; Davidson, I. J. *J. Electrochem. Soc.* **2010**, *157*, A528.
(13) Ulvestad, A.; Cho, H. M.; Harder, R.; Kim, J. W.; Dietze, S. H.; Fohtung, E.; Meng, Y. S.; Shpyrko, O. G. *Appl. Phys. Lett.* **2014**, *104*, 073108.
(14) Kim, J.-H.; Yoon, C. S.; Myung, S.-T.; Prakash, J.; Sun, Y.-K. *Electrochem. Solid-State Lett.* **2004**, *7*, A216−A220.
(15) Kim, J.-H.; Myu, S.; Yoon, C. S.; Ka, S. G.; Su, Y.; Myung, S.-T.; Kang, S. G.; Sun, Y.-K. *Chem. Mater.* **2004**, *16*, 906−914.
(16) Lee, E.; Persson, K. a. *Energy Environ. Sci.* **2012**, *5*, 6047−6051.
(17) Malik, R.; Zhou, F.; Ceder, G. *Nat. Mater.* **2011**, *10*, 587−590.
(18) Kunduraci, M.; Amatucci, G. G. *Electrochim. Acta* **2008**, *53*, 4193−4199.
(19) Yang, M.-C.; Xu, B.; Cheng, J.-H.; Pan, C.-J.; Hwang, B.-J.; Meng, Y. S. *Chem. Mater.* **2011**, *23*, 2832−2841.
(20) Padhi, A. K. *J. Electrochem. Soc.* **1997**, *144*, 1188−1194.
(21) Cogswell, D. A.; Bazant, M. Z. *ACS Nano* **2012**, *6*, 2215−2225.
(22) Chen, G.; Song, X.; Richardson, T. J. *Electrochem. Solid-State Lett.* **2006**, *9*, A295.
(23) Delmas, C.; Maccario, M.; Croguennec, L.; Le Cras, F.; Weill, F. *Nat. Mater.* **2008**, *7*, 665−671.
(24) Sharma, N.; Guo, X.; Du, G.; Guo, Z.; Wang, J.; Wang, Z.; Peterson, V. K. *J. Am. Chem. Soc.* **2012**, *134*, 7867−7873.
(25) Holtz, M. E.; Yu, Y.; Gunceler, D.; Gao, J.; Sundararaman, R.; Schwarz, K. A.; Arias, T. A.; Abruña, H. D.; Muller, D. A. *Nano Lett.* **2014**, *14*, 1453−1459.
(26) Bai, P.; Cogswell, D. A.; Bazant, M. Z. *Nano Lett.* **2011**, *11*, 4890−4896.
(27) Warren, B. E. *X-ray Diffraction*; Courier Dover Publications: New York, 1969; p 381.

(28) Pfeifer, M. A.; Williams, G. J.; Vartanyants, I. A.; Harder, R.; Robinson, I. K. *Nature* **2006**, *442*, 63−66.
(29) Vartanyants, I. A.; Robinson, I. K. *J. Phys.: Condens. Matter* **2001**, *13*, 10593.
(30) Dreyer, W.; Jamnik, J.; Guhlke, C.; Huth, R.; Moskon, J.; Gaberscek, M. *Nat. Mater.* **2010**, *9*, 448−453.
(31) Cahn, J. W. *Acta Metall.* **1961**, *9*, 795−801.
(32) Chang, H.-H.; Chang, C.-C.; Wu, H.-C.; Yang, M.-H.; Sheu, H.-S.; Wu, N.-L. *Electrochem. Commun.* **2008**, *10*, 335−339.
(33) Shin, H. C.; Chung, K. Y.; Min, W. S.; Byun, D. J.; Jang, H.; Cho, B. W. *Electrochem. Commun.* **2008**, *10*, 536−540.
(34) Liu, H.; Strobridge, F. C.; Borkiewicz, O. J.; Wiaderek, K. M.; Chapman, K. W.; Chupas, P. J.; Grey, C. P. *Science* **2014**, *344*, 1252817.
(35) Niu, J.; Kushima, A.; Qian, X.; Qi, L.; Xiang, K.; Chiang, Y.-M.; Li, J. *Nano Lett.* **2014**, *14*, 4005−4010.
(36) Cogswell, D. A.; Bazant, M. Z. *Nano Lett.* **2013**, *13*, 3036−3041.

dx.doi.org/10.1021/nl502332b | *Nano Lett.* XXXX, XXX, XXX−XXX